Phonon Propagation in Ordered Diblock Copolymer Solutions

G. Tommaseo,[†] R. S. Penciu,[‡] G. Fytas,*[,†,‡] E. N. Economou,[‡] T. Hashimoto,[§] and N. Hadjichristidis[||]

Max Planck Institute of Polymer Research, P.O. Box 3148, 55128 Mainz, Germany, FORTH/Institute of Electronic Structure and Laser, P.O. Box 1527, 71110 Heraklion, Greece, Department of Polymer Chemistry Graduate School of Engineering, Kyoto University, Kyoto 6158510 Japan, and Department of Chemistry, University of Athens, 15701 Zografou, Athens, Greece

Received February 25, 2004; Revised Manuscript Received April 16, 2004

ABSTRACT: High-resolution inelastic light scattering was employed to measure the dispersion relations for the acoustic excitations in ordered concentrated solutions of poly(styrene)-*block*-poly(isoprene) copolymers with both symmetric and asymmetric composition and large spacing (220−415 nm). The morphology is manifested in the rich phonon spectrum recorded for different scattering wave vectors **q** in the range 0.003−0.034 nm^{-1}. The experimental $\omega_s(q)$ of the *s*th branch is directly compared with the theoretical dispersion from band structure calculations performed for different directions of **q** in the reciprocal lattice of lamellar and cylindrical periodic structures. The dispersion relations turn out to be a sensitive index of the microphase morphology and the grain orientation.

I. Introduction

Acoustic/elastic excitations in the GHz frequency range can sensitively be probed by inelastic (Brillouin) light scattering at low wave vectors **q** in the range 0.003−0.035 nm^{-1}. In homogeneous media, the experimental spectrum $I(q,\omega)$ displays one Brillouin doublet at a frequency $\pm cq$ on both sides of the elastic Rayleigh peak. This doublet corresponds to the acoustic phonon of wave vector $\mathbf{k} = \mathbf{q}$ with c being the phase velocity of the sound in the average isotropic medium. Even for microphase-separated diblock copolymers with short spacing $d = 20$ nm, Brillouin scattering reveals only this single acoustic phonon.[1] For inhomogeneous media, however, over a characteristic length $d = O(q^{-1})$ additional modes can, in principle, be observed through the mixing of q with k and the reciprocal lattice vector due to the interaction of light with phonons and the periodic lattice.[2]

On the basis of a recent report,[2] a lamellar forming long diblock copolymer with photonic stop band in the visible spectrum ($d \gg 180$ nm) can exhibit a Bragg mode, reflecting the spacing of the layered structure, an optic-like mode, reflecting the morphological characteristics, and the acoustic phonon of the average medium. The relative strength of the first two modes depends on the lamellae orientation relative to the probing scattering vector **q**. The phonon spectrum extends over the edge of the first Brillouin zone, and extension to high orders is feasible for long spacing, i.e., longer diblock copolymer chains. Application of the technique to different mesoscopic structures, e.g., cylindrical or spherical morphologies, is also missing.

To address large lamellar spacing and cylindrical microstructures, we report here on Brillouin scattering spectra of ordered solutions of ultrahigh molar mass M_w symmetric ($f_s = 0.49$, $M_w = 3.6 \times 10^6$ g/mol) and two asymmetric ($f_s = 0.83$, $M_w = 1.6 \times 10^6$ g/mol and $f_s = 0.24$, $M_w = 1.93\ 10^6$ g/mol) poly(styrene)-*block*-poly(isoprene)(SI) with poly(styrene) (PS) composition f_s. Detailed synthetic procedures and molecular characterization are given elsewhere.[4] The appearance of the rich phonon spectrum sensitively relates to the morphology, the spacing, and the orientation of **q** relative to the unit cell of the ordered solutions. Hence, even for the present polycrystalline systems the fine phonon structure of an ideal crystalline material can be traced through cell orientation relative to **q**. This somewhat tedious procedure leads, however, to the phonon dispersion relations that compares well with the theoretical dispersion relations for a given morphology at certain q−lattice orientations.

II. Experimental Section

Polarized Rayleigh−Brillouin spectra $I(q,\omega)$ arising from thermal density fluctuations in the system at equilibrium were recorded at different scattering angles θ by a six-pass tandem Fabry−Perot interferometer (FPI) using the setup described elsewhere.[3] The inelastic light scattering involves photons of incoming, $\mathbf{k_i}$, and outgoing, $\mathbf{k_s}$, wave vectors scattered by phonons of wave vector **k** and possibly by the periodic lattice which adds a reciprocal lattice vector **G**, so that $\mathbf{q} = \mathbf{k_i} - \mathbf{k_s} \equiv \mathbf{k} + \mathbf{G}$. The magnitude of the photon scattering wave vector is $|\mathbf{q}| = (4\pi n/\lambda)\sin(\theta/2)$ with $\lambda = 532$ nm being the wavelength of the single-mode solid-state laser and n (=1.59) is the refractive index of the medium. The light scattering cells were NMR tubes with 5 mm outer diameter.

The three diblock copolymers used are poly(styrene)-*block*-poly(isoprene) diblock copolymers with different styrene composition f_s and weight-average molar mass M_w (g/mol): SI4M50 with $f_s = 0.5$ and $M_w = 3.6 \times 10^6$, SI2M20 with $f_s = 0.24$ and $M_w = 1.93 \times 10^6$, and SI2M80 with $f_s = 0.83$ and $M_w = 1.6 \times 10^6$. Solutions of these SI in toluene undergo[4] the well-known disorder to order transition (ODT) above a critical SI concentration w_{ODT} which ranges from 4.2 (for the SI4M50) to 9.2 wt % (for the SI2M80) at 20 °C. The two asymmetric SI clearly form hexagonally arranged cylinders (of either PS or PI) above w_{ODT}, as shown by the TEM image of an annealed SI2M20 film when the specimen films are cast with a neutral solvent such as toluene in Figure 1.The ordered structures in solution of the two asymmetric SI with toluene as a solvent should also be hexagonal cylinders. For the symmetric

* To whom correspondence should be addressed. E-mail: fytas@iesl.forth.gr.
[†] Max Planck Institute of Polymer Research.
[‡] FORTH/Institute of Electronic Structure and Laser.
[§] Kyoto University.
[||] University of Athens.

10.1021/ma0496246 CCC: $27.50
Published on Web 05/22/2004

Figure 1. TEM image for a toluene cast and annealed film of the asymmetric poly(styrene)-*block*-poly(isoprene) SI2M20 showing cylinders of PS in the PI matrix.

SI4M50/toluene system, the light scattering intensity profile displays the first-order diffraction peak from the corresponding spacing of 355 nm. Judging from $f_{PS} = 0.5$ and neutral solvent used, the ordered solution is expected to have lamellar morphology.

III. Results and Discussion

A. Symmetric Diblock Copolymer. For the symmetric SI4M50, two concentrations above $w_{ODT} = 4.2$ wt % were considered. The experimental $I(q,\omega)$ at $q = 0.025$ nm^{-1} ($\theta = 90°$) in Figure 2a recorded for two different orientations relative to the incident laser beam demonstrate the anisotropy of the ordered solution with $d = 355$ nm at 20 °C. Clearly $I(q,\omega)$ depends on the grain orientation in the probed volume. Usual inspection of the sample shows large reflective grains, and the orientation dependence in Figure 2a suggests grain sizes on the order of the probed volume (~100 μm diameter). Due to the large spacing even at low q (0.006 nm^{-1}), the $I(q,\omega)$ in Figure 2b displays rich structure. The frequency of the acoustic phonon (1) in Figure 2 clearly increases with q.

The frequency of the Brillouin peaks quantitatively allocated from the representation of the experimental spectra by the superposition of the necessary (up to five) Lorentzians is plotted in Figure 3 as a function of the scattering wave vector q. In this dispersion plot the acoustic (square symbols) mode $\omega = cq$ yields the longitudinal phase velocity of sound in a homogeneous fluid where $\omega = 2\pi f$ and f is the frequency in GHz. The speed $c = 1380$ m/s is expectedly close to the value in the solvent toluene since PS and PI microdomains are well swollen by the majority solvent component. Below 0.02 nm^{-1} the dispersion plot looks qualitatively the same as that of a lamellar ordered 17 wt % solution of lower M_w (1.04 10^6 g/mol) SI1M50 in toluene (Figure 3 in ref 2) which displays the Bragg (2) (triangles) and the "optic like" (solid circles) phonons in Figure 3. Due to the small contrast between the two microphases, the frequency of the Bragg mode was well described by the approximate relation[2]

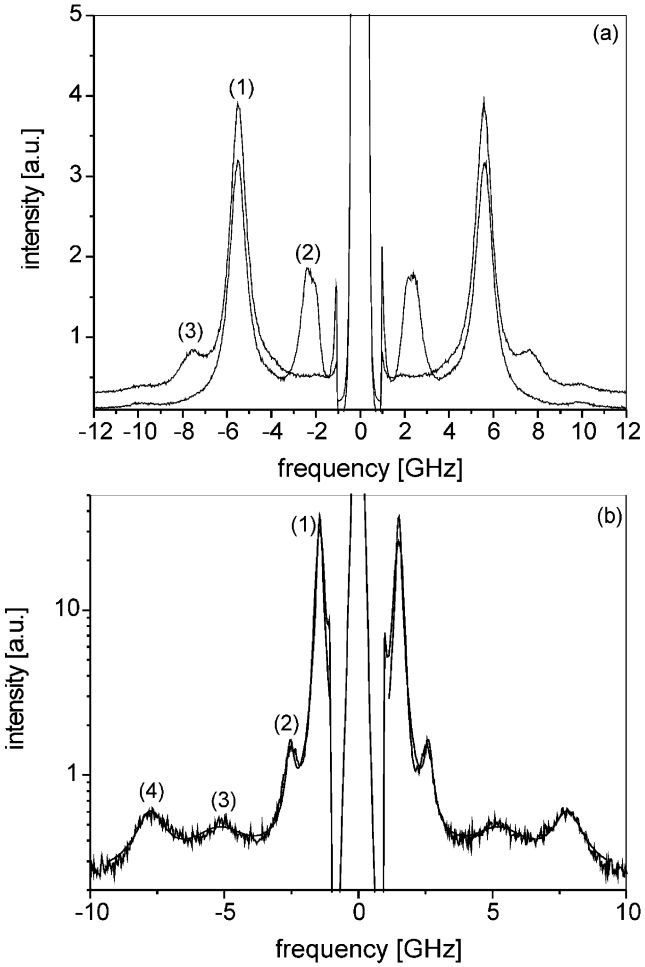

Figure 2. Rayleigh−Brillouin spectra of the SI4M50/toluene ordered solution at $q = 0.025$ (a) and 0.006 nm^{-1} (b) at 20 °C. The rich phonon spectrum is represented by the superposition of Lorentzians (solid lines in b). The spectrum of the same solution (part a) depends on the orientation relative to the laser beam that strongly affects the intensity of modes 2 and 3 but not the intensity and frequency of the acoustic phonon 1.

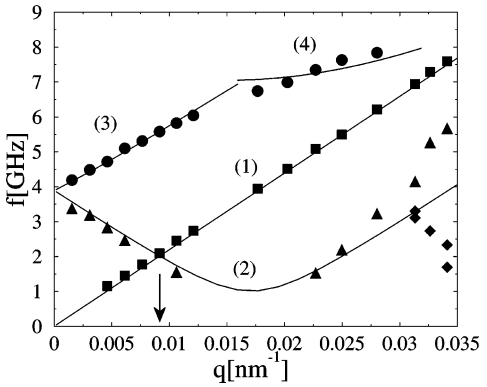

Figure 3. Phonon dispersion relations for the ordered SI4M50 solution. The solid points and the lines are the experimental and theoretical frequencies of the different modes. The latter are obtained for $d = 355$ nm, $c = 1380$ m/s, and $\alpha = 75°$ (2), 50° (3), and 35° (4). The acoustic phonon (1) is expectedly present at all values of a. The arrow indicates the edge of the first Brillouin zone.

$$\omega = c(G - k_z) \quad (1)$$

where $G = 2\pi/d$ is the magnitude of the one-dimensional lattice vector and $k_z = q \sin \alpha$ the component of **q** perpendicular to the lamellae with α being the angle between **q** and the lamellar plane. The strength of this mode in the experimental spectra is therefore orientation dependent (Figure 2a) and absent for α = 0°. Hence, the resemblance to the Bragg diffraction conditions suggests the name of this mode.

On the basis of eq 1, $f = c/d$ at $q = 0$, the Bragg (2) and acoustic (1) phonon frequencies cross at $q = \pi/d$, i.e., at the edge of the first Brillouin zone, and the propagation ceases at $q = G$. With $d = 355$ nm, eq 1 represents the present situation in the first Brillouin zone very well. This large spacing allows the probing of higher Brillouin zones and the observation of additional phonons which add to the sensitivity of the technique for structure characterization.

For certain cell orientations, two branches emerge in the low-*f* high-*q* range of the dispersion plot which were apparently absent in the SI1M50 solutions (Figure 3, ref 2). Phononic band structure calculations of a lamellar morphology with $d = 355$ nm and $c = 1380$ m/s leads to the solid lines in Figure 3 for three values of α. The computed Bragg mode for α = 75° (eq 2 below) is single and describes mode 2 in the first Brillouin zone well but is lower than the experimental frequency of this mode at higher *q*'s. Concurrently, the dispersion of the highest frequency mode (3 and 4 in Figure 3) is convex, in contrast to the concave form of this mode in SI1M50 ordered solutions. For low mechanical mismatch, this high-frequency mode with weak dispersion associated with displacements within the layered structure is given[2] by

$$\omega = c((G - k_z)^2 + k^2_{xy})^{1/2} \quad (2)$$

where $k_{xy} = q \cos \alpha$ and the predicted dispersion has a concave and not convex form. For SI1M50 lamellar solutions, good agreement between experiment and eq 2 was achieved[2] with a value of α ≈ 15°. In the present case of SI4M50, two values of α (50° for 3 and 35° for 4) are needed in order to achieve a reasonable description of this branch. However, at $q = 0$, the frequencies of this third branch and the Bragg mode are predicted (eq 2) and experimentally observed (Figure 3) to coincide at $f = c/d$. The phonons at the high-*q* and low-*f* region are not theoretically predicted for lamellar structures using a single α value. These phonons are, however, theoretically found for different values of α (eq 2).

The partial agreement between the theoretical and experimental dispersion of Figure 3 might be due to slight deviation from an ideal lamellar morphology as indicated by the position of the second-order peak in the light scattering intensity profile of the ordered SI4M50/toluene solution. On the experimental side, we confirmed the measured dispersion relations for a higher concentration of the SI4M50/toluene system and hence for $d = 415$ nm and $c = 1405$ m/s. Figure 4 depicts this situation in the reduced fd/c vs qd plot, where the good superposition deteriorates at high qd values for the Bragg mode.

B. Asymmetric Diblock Copolymers. In the case of 2D structures, in addition to angle α the orientations of **q** in the plane perpendicular to cylinder axes are not equivalent and the phonon spectrum of the ordered

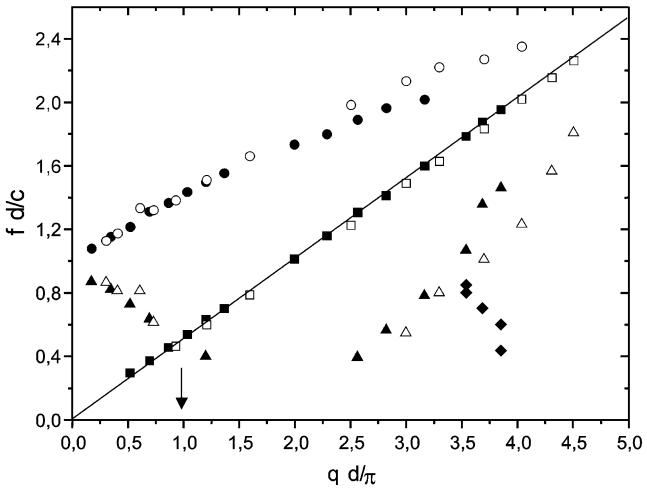

Figure 4. Reduced experimental dispersion relations in two ordered SI4M50 solutions with $d = 355$ nm, $c = 1380$ m/s and $d = 415$ nm, $c = 1405$ m/s. The arrow indicates the edge of the first Brillouin zone.

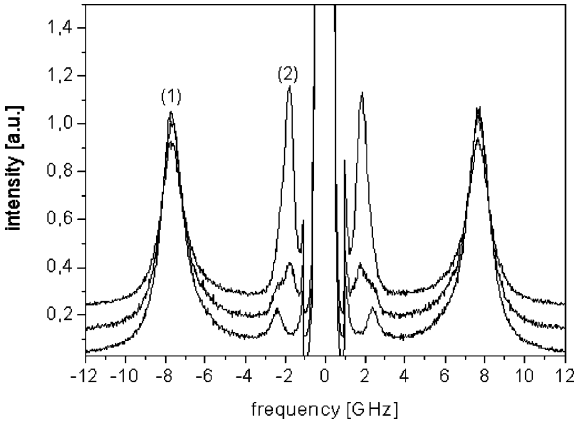

Figure 5. Rayleigh−Brillouin spectra of 9.6 wt % SI2M20/toluene ordered solution at $q = 0.0335$ nm^{-1}. As in Figure 2, the spectra of the same solution depend on the orientation of the cell relative to the laser beam as shown for three orientations.

solutions of the asymmetric diblock copolymers should be strongly anisotropic. This behavior is displayed by the ordered solutions of SI2M20 ($w_{ODT} = 7.4$ wt %) and SI2M80 ($w_{ODT} = 9.2$ wt %) in toluene. Figure 5 shows Rayleigh−Brillouin spectra for the 9.6 wt % SI2M20/toluene ordered solution at 0.0335 nm^{-1} at three cell orientations at 20 °C. Only the acoustic phonon (1) (at 7.7GHz) is expectedly insensitive to the probed scattering volume, whereas the other peaks, in particular in the low-frequency region of the spectrum, change dramatically. The phonon spectra of the 15 wt % SI2M80/toluene ordered solution exhibits similar behavior, which will be discussed in terms of the dispersion relations below.

Figure 6a shows the dispersion relations for the SI2M20 system obtained at different cell orientations. For the Bragg phonons (2) with negative dispersion at $q > 0.02$ nm^{-1}, not only the intensity but also the frequency were found to depend on the orientation, resulting in different experimental frequencies in Figure 6a. In particular, the systematic variation is larger near the minimum of the lowest frequency at ca. 0.027 nm^{-1}. Over the same *q* range, the second higher frequency Bragg mode (2′) (right triangles in Figure 6a), which was absent in SI4M50 (Figure 3), is not observed

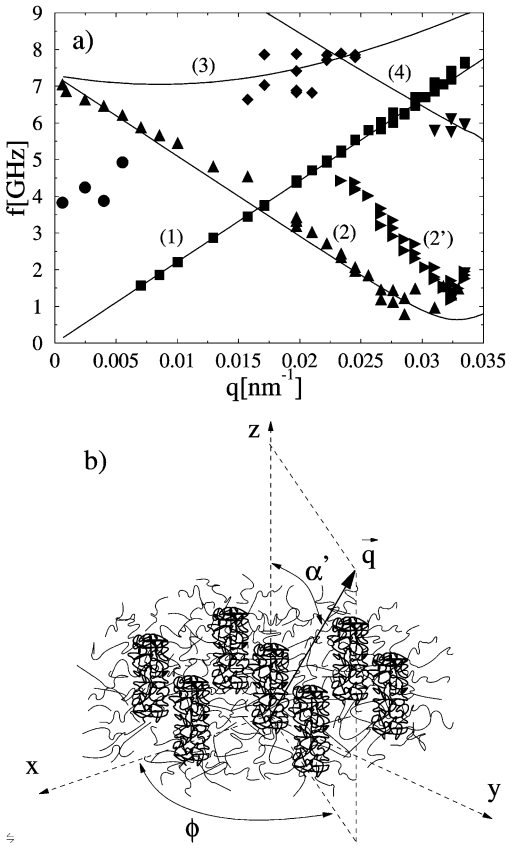

Figure 6. (a) Phonon dispersion relations for the ordered SI2M20 solution ($d = 220$ nm, $c = 1390$ m/s). The solid points and lines denote the experimental and theoretical frequencies of the different modes: $\alpha' = 90°$, $\phi = 5°$ is for 2, whereas $\alpha' = 0°$, $\phi = 15°$ is for branches 3, 4. Branch 1 is the same for all combinations of α' and ϕ. The arrow indicates the edge of the first Brillouin zone. (b) Definition of the orientation angles α' and ϕ in the unit cell of the hexagonally arranged cylinders.

concurrently with the lower frequency mode (2). Hence, these two modes should correspond to different grain orientation relative to **q**.

The theoretical band structure calculations were performed using the well-known plane-wave scattering method.[2,5] This fast method is based on expansion of the periodic coefficients in the elastic wave equation in Fourier series. It applies to cases where both scatterers and host are either fluids or solids.

The dispersion relations for hexagonally arranged cylinders now depend on two angles: on the angle α' between **q** and the cylinders (*z*-axis) and on the angle *f* in the plane perpendicular to the hexagonally arranged cylinders as schematically shown in Figure 6b. In this case the corresponding expressions of eqs 1 and 2 read

$$\omega = c|\mathbf{G} - \mathbf{k}_{xy}| \tag{3}$$

where **G** belongs to the $x-y$-plane with $G_x = n_1 2(\pi/d)$ and $G_y = 2(\pi/\sqrt{3}d)(2n_2 - n_1)$ (n_1, n_2 being integer numbers) and

$$\omega = c((G_x - k_x)^2 + (G_y - k_y)^2 + k^2{}_x)^{1/2} \tag{4}$$

For $\alpha' = 90°$, the theoretical dispersions for $\phi = 0°$ and 30° are distinctly different and could be experimentally distinguished. On the other hand, for $\alpha' = 60°$ and 30° there are no low-frequency phonons at high *q*, in contrast to the experimental dispersion of Figure 6a. The solid lines in Figure 6a are theoretical dispersion relations for $d = 220$ nm and different values for the two angles α' and ϕ which capture the observed modes except the branch (2′) (right triangles in Figure 6a). We recall that the latter corresponds to different grain orientation relative to *q*.

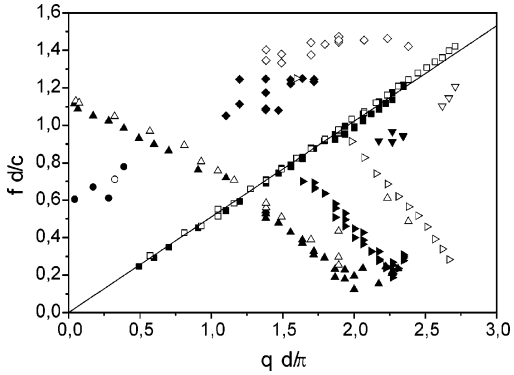

Figure 7. Reduced experimental dispersion relations for the two ordered SI2M20 ($d = 220$ nm, solid symbols) and SI2M80 ($d = 254$ nm, open symbols) solutions.

The Bragg mode (2) can be represented by $\alpha' = 90°$ and $\phi = 5°$, while the somewhat higher $\phi = 15°$ is needed to capture branches 3 and 4 (see eq 4). There is no combination of orientation angles $0 \le \alpha' \le 90°$ and $0 \le \phi \le 30°$ that can predict the experimental branches 2 and 2′ simultaneously. The points which are denoted by 2′ cannot be captured by restricting *q* to any fixed direction. Instead, its frequency can be well represented (eq 3) by varying the angle $10° \le \phi \le 30°$ and keeping $\alpha' = 90°$. This remarkable sensitivity of this mode to the angle *f* (see Figure 6b) might reflect the large fluctuations in the angular correlations of the cylinders in the $x-y$-plane as indicated by the TEM image (Figure 1). Alternatively, the weaker fluctuations in the average intercylinder distance *d* rationalize the stability of branch 2.

On the theoretical side, in the calculations the finite radius R_c (~60 nm) of cylinders was irrelevant due to the very small difference in the elastic constants and densities inside and outside the cylinders. In fact, the absence of band gaps in the dispersion plot and the characteristic optic-like mode due to cylinder vibrations[3,6–8] indicates sufficiently small elastic constant contrast. On the experimental side, the validity of this reasonable assumption and the role of the two lengths in the phonon dispersion can be further examined by reversing the material between the core and matrix of the ordered solutions. The 2 and 2′ frequencies in SI2M80 and SI2M20 with almost mirror compositions should reveal the dependence on either or both length scales *d* and R_c.

In SI2M80, the PI component now forms the cylinders and the PS block lies in the matrix and both microdomains are solvated by the solvent toluene. Figure 7 displays the experimental dispersions for the 15 wt % SI2M80 ($d = 254$ nm) and 9.6 wt % SI2M20 ($d = 220$ nm) ordered solutions in the reduced plot fd/c vs qd with $c = 1390$ m/s. The overall good superposition suggests the relevance of the intercylinders distance and similar grain orientation in the two systems. Branch 2′ is, however, distinguished taking higher frequency in the SI2M80 system (right open triangles) at constant qd. The lack of superposition for 2′ in the two systems might

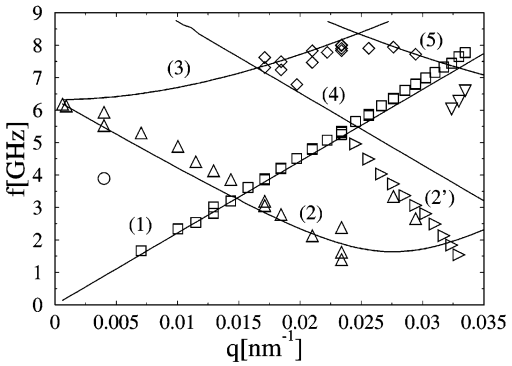

Figure 8. Phonon dispersion relations for the ordered SI2M80 solution. The solid points and lines denote the experimental and theoretical (d = 254 nm, c = 1390 m/s; $\alpha = 90°$ and $\phi = 15°$ for 2 and $\alpha' = 90°$ and $\phi = 30°$ for 3 and 4) frequencies. Branch 1 is the same for all combinations of α' and ϕ.

hint at the importance of the orientation fluctuations in the cylinder axes.

For SI2M80, the comparison with the theoretical dispersion using d = 254 nm, $\alpha' = 90°$, and different values for f is shown in Figure 8. The Bragg mode (2) is represented by $\phi = 15°$, whereas the other modes can relate to branches 3−5 computed with $\phi = 30°$. Although branch 4 shows some resemblance to the experimental 2′, again this mode cannot be described by a single direction of **q**. Instead, an almost monotonic variation of f between 15° and 30° can represent the experimental frequencies of 2′ over the q range 0.024−0.034 nm^{-1} (see eq 3).

IV. Concluding Remarks

Brillouin spectroscopy is a nondestructive inelastic light scattering technique offering accurate access to the dispersion relation in soft materials ordered in the submicrometer range. Because of the low contrast between the elastic constants and the densities of the microphases, we obtained simple analytical ω vs **q** relations which satisfactorily describe the interaction of light with phonons and the periodic lattice. The rich phonon spectrum of three ordered diblock copolymer solutions depends not only on the geometrical characteristics but also on the orientation of the subdomains relative to the scattering wave vector.

Polycrystallinity does not prevent the application of the technique. Instead, detailed morphological insight is feasible through the theoretical description of the experimental dispersion relation. For example, the orientation of the cylinders in the asymmetric diblock copolymers manifests itself in the phonon dispersion plot. The complementary inelastic X-ray scattering technique[9,10] at shorter wavelengths and hence in the THz frequency range exhibits lower resolution as compared to the Brillouin light scattering due to the inherently broad phonon spectra.

References and Notes

(1) Floudas, G.; Steffen, W.; Hadjichristidis, N. *Europhys. Lett.* **1998**, *44*, 37.
(2) Urbas, A.; Thomas, E. L.; Kriegs, H.; Fytas, G.; Penciu, R. S.; Economou, E. N. *Phys. Rev. Lett.* **2003**, *90*, 108302.
(3) Penciu, R. S.; Kriegs, H.; Petekidis, G.; Fytas, G.; Economou, E. N. *J. Chem. Phys.* **2003**, *118*, 5224.
(4) Holmqvist, P.; Pispas, S.; Hadjichristidis, N.; Fytas, G.; Sigel, R. *Macromolecules* **2003**, *36*, 830.
(5) Economou, E. N.; Sigalas, M. M. *J. Acoust. Soc. Am.* **1994**, *95*, 1734.
(6) Duval, E.; Boukenter, A.; Champagnon, B. *Phys. Rev. Lett.* **1986**, *56*, 2052.
(7) Liu, J.; Je, K.; Weitz, D. A.; Sheng, P. *Phys. Rev. Lett.* **1990**, *65*, 2802.
(8) Penciu, R. S.; Fytas, G.; Economou, E. N.; Steffen, W.; Yannopoulos, S. N. *Phys. Rev. Lett.* **2000**, *85*, 4622.
(9) Chen, S.; Liao, C.; Huang, H.; Weiss, T.; Belliscent, M. C.; Sette, F. *Phys. Rev. Lett.* **2001**, *86*, 740.
(10) Kriegs, H.; Steffen, W.; Fytas, G.; Monaco, G.; Dreyfus, C.; Fragouli, P.; Pitsikalis, M.; Hadjichristidis, N. *J. Chem. Phys.*, in press.

MA0496246